

Microscopic model of the doping dependence of linewidths in monolayer transition metal dichalcogenides

Cite as: J. Chem. Phys. **152**, 194705 (2020); <https://doi.org/10.1063/5.0008730>

Submitted: 25 March 2020 . Accepted: 30 April 2020 . Published Online: 20 May 2020

 Matthew R. Carbone, Matthew Z. Mayers, and  David R. Reichman

COLLECTIONS

Paper published as part of the special topic on [2D Materials](#)



View Online



Export Citation



CrossMark

ARTICLES YOU MAY BE INTERESTED IN

[Optical properties of charged excitons in two-dimensional semiconductors](#)

The Journal of Chemical Physics **153**, 034703 (2020); <https://doi.org/10.1063/5.0012475>

[Ground and excited state exciton polarons in monolayer MoSe₂](#)

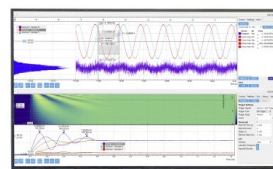
The Journal of Chemical Physics **153**, 071101 (2020); <https://doi.org/10.1063/5.0013092>

[Light-matter coupling and non-equilibrium dynamics of exchange-split trions in monolayer WS₂](#)

The Journal of Chemical Physics **153**, 034706 (2020); <https://doi.org/10.1063/5.0012721>

Challenge us.

What are your needs for
periodic signal detection?



Zurich
Instruments

Microscopic model of the doping dependence of linewidths in monolayer transition metal dichalcogenides

Cite as: J. Chem. Phys. 152, 194705 (2020); doi: 10.1063/5.0008730

Submitted: 25 March 2020 • Accepted: 30 April 2020 •

Published Online: 20 May 2020



View Online



Export Citation



CrossMark

Matthew R. Carbone,^{a)}  Matthew Z. Mayers, and David R. Reichman^{b)} 

AFFILIATIONS

Department of Chemistry, Columbia University, New York, New York 10027, USA

Note: This paper is part of the JCP Special Topic on 2D Materials.

^{a)} Author to whom correspondence should be addressed: mrc2215@columbia.edu

^{b)} Electronic mail: drr2103@columbia.edu

ABSTRACT

A fully microscopic model of the doping-dependent exciton and trion linewidths in the absorption spectra of monolayer transition metal dichalcogenides in the low temperature and low-doping regime is explored. The approach is based on perturbation theory and avoids the use of phenomenological parameters. In the low-doping regime, we find that the trion linewidth is relatively insensitive to doping levels, while the exciton linewidth increases monotonically with doping. On the other hand, we argue that the trion linewidth shows a somewhat stronger temperature dependence. The magnitudes of the linewidths are likely to be masked by phonon scattering for $T \geq 20$ K in encapsulated samples in the low-doping regime. We discuss the breakdown of perturbation theory, which should occur at relatively low-doping levels and low temperatures. Our work also paves the way toward understanding a variety of related scattering processes, including impact ionization and Auger scattering in clean 2D samples.

Published under license by AIP Publishing. <https://doi.org/10.1063/5.0008730>

I. INTRODUCTION

Monolayer transition metal dichalcogenides (TMDCs) are quasi-two-dimensional materials known to exhibit extraordinary physical phenomena.^{1,2} These materials may be viewed as semi-conducting analogs of graphene^{3–5} and present with non-trivial optical, electronic, and, under some circumstances, topological and superconducting properties.^{6,7} Due to their unique characteristics, monolayer TMDCs have been proposed for myriad practical applications⁸ such as opto-electronics,^{9–12} field-effect transistors,¹³ and digital logic gates.^{14,15} Of particular fundamental interest is the nature of electron–hole complexes such as excitons^{16,17} and trions^{18,19} in TMDCs. Due to the reduced screening in two-dimensional (2D) systems, such stable carrier complexes may have anomalously large binding energies, with that of the exciton reaching ~ 0.5 eV^{16,20–22} and that of the trion reported to be in the range of 20–35 meV,^{18,21,23–25} implying that trions are bound even at room temperature. These observations indicate that monolayer TMDCs are unique systems for investigating the properties of strongly

interacting quasiparticles. In addition, they may provide unprecedented experimental clarity concerning the nature of interactions between these electron–hole complexes and phonons^{26,27} as well as with charge carriers and other quasiparticles.

A standard means of probing the nature of the interactions of excitons and trions with other excitations is via the broadening of linewidths in clean samples with respect to control parameters such as the temperature or carrier density. Intrinsic homogeneous quasiparticle (QP) linewidths²⁶ are generally obfuscated by inhomogeneous broadening due to the high level of static defects in processing. However, recent work has led to the observation of very narrow QP linewidths via the preparation of ultra-clean samples by both dry transfer methods and chemical vapor deposition^{28–30} and by the usage of non-linear spectroscopy to extract the homogeneous linewidth from inhomogeneously broadened spectra.²⁶ The optical interrogation of the exciton and trion linewidths in these less defective samples offers a unique opportunity to understand the mechanisms of the 2D exciton and trion scattering processes in quasi-2D systems.

There are many factors that affect line broadening in monolayer TMDCs, most notably interactions with phonons (as controlled by temperature) and interactions with other charge carriers (as controlled by doping). At very low temperatures and near the charge-neutrality point,²⁷ it is expected that the intrinsic homogeneous linewidth due to lifetime broadening may be observed if the sample is clean enough. As temperature increases, phonons begin to play a significant role and will eventually dominate the line broadening process. The interaction of excitons with phonons has been studied in some detail in TMDCs,^{27,31} and a variety of coupling motifs have been elucidated experimentally and theoretically.

Additionally, the concentration of electrons as controlled by gating can alter linewidths and line shapes in a non-trivial fashion.^{16,32–34} Studies that have investigated the electron density dependence of optical line shapes in monolayer TMDCs from the Fermi-polaron perspective provide a means of describing optical line broadening as a function of doping.^{35–41} Such many-body multiple scattering theories are essential for properly describing the full range of doping-dependent behavior, as the Fermi golden rule breaks down at sizable doping levels. However, the use of graphene gating and clean samples renders the investigation of the doping regime close to the charge-neutrality point possible.⁴² Here, detailed microscopic golden rule-based calculations that can provide new insights into the line broadening mechanisms may be performed. Motivated by the aforementioned recent experimental works, we follow this latter path to assess how the elastic scattering of excitons and trions with free charge carriers may alter linewidths of both ground and excited state excitonic complexes in the low-doping regime. In particular, we investigate the circumstances for which doping-related broadening may compete with phonon-induced broadening, and we discuss the breakdown of the perturbative approach as a function of temperature and carrier density. The importance of our work extends beyond the description of linewidths and is of relevance for describing scattering processes such as Auger recombination and impact ionization in TMDCs.

Our paper is organized as follows: We first present an outline of the microscopic theory in Sec. II, focusing on the electron-exciton scattering calculation, which is discussed in Subsection II A. Calculations for the electron-trion scattering are similar to that of the exciton and discussed (briefly) in Subsection II B. The low-temperature results for the trion and exciton linewidths, in addition to the details of the model and limitations of the golden rule approach, are presented and discussed in Sec. III. Finally, in Sec. IV, we summarize our conclusions and discuss outlook and potential future work. Details not contained in the main text are located in several appendixes.

II. METHODOLOGY

In this section, the elastic (energy-conserving) scattering of electrons from both excitons and trions are described within the Fermi golden rule approximation. Additionally, because we work at the golden rule level of theory, bound states in scattering are not considered. While such a treatment can only be valid at extremely low doping densities, recent synthetic work using encapsulated samples points to a route to experimentally controlled access to this regime. Furthermore, the use of the golden rule allows for a very

detailed microscopic description,^{43,44} the limitations of which will be discussed in the following sections.

A. Electron-exciton elastic scattering

In order to facilitate the computation, we use a simple variational guess for the exciton wave function

$$\phi(r) = \sqrt{\frac{\pi}{2\lambda^2}} e^{-r/\lambda}, \quad (1)$$

where r is the relative coordinate of the two-body system. The optimal effective Bohr radius λ is chosen to best match the functional form of (1) to the ground state of a Wannier exciton in a Rytova-Keldysh potential^{45,46} found using exact diagonalization.

The second-quantized form of the exciton-free electron scattering state is

$$|\mathbf{k}_x, \mathbf{k}_e\rangle = \sum_{\mathbf{k}'} \phi_{\alpha_x \mathbf{k}_x + \mathbf{k}'}^* \psi_{\mathbf{k}_e}^* c_{-\mathbf{k}'}^\dagger d_{\mathbf{k}_x + \mathbf{k}'}^\dagger c_{\mathbf{k}'}^\dagger |0\rangle, \quad (2)$$

which is a direct product state of the free exciton and electron states, $|\mathbf{k}_x\rangle \otimes |\mathbf{k}_e\rangle$. The wave function

$$\phi_{\mathbf{k}} = \sqrt{\frac{8\pi\lambda^2}{A}} g(\lambda k) \quad (3)$$

satisfies normalization $\sum_{\mathbf{k}} \phi_{\mathbf{k}}^2 \rightarrow \frac{A}{(2\pi)^2} \int d^2k \phi_{\mathbf{k}}^2 = 1$ and is derived by performing an in-plane Fourier transform of (1), where $g(x) = [1 + x^2]^{-3/2}$, $c_{\mathbf{k}}$ ($d_{\mathbf{k}}$) are electron (hole) annihilation operators for momentum index \mathbf{k} , A is the in-plane area of the 2D material, and $\alpha_x = m_e/M_x$ is the ratio of the electron and exciton effective masses (which manifests during the coordinate transform to relative/center of mass coordinates). The free-electron wave function $\psi_{\mathbf{k}} \propto e^{-i\mathbf{k}\cdot\mathbf{R}}$ characterizes an electron that may exhibit free in-plane motion and together with the center of mass coordinate of the exciton, contributes only a global phase factor that may be ignored in subsequent calculations, as it does not contribute to the determination of the scattering rate.

Scattering matrix elements are computed by evaluating the coupling between an initial QP-free electron state, $|\mathbf{k}_x, \mathbf{k}_e\rangle$, and a final QP-free electron state in which momentum \mathbf{q} is transferred, $\langle \mathbf{k}_x + \mathbf{q}, \mathbf{k}_e - \mathbf{q} |$. The second-quantized, momentum-conserving potential energy operator $V = V_{eh} + V_{ee}$ that mediates this coupling may be split into electron-hole and electron-electron components,

$$V_{eh} = - \sum_{\substack{\mathbf{k}_1, \mathbf{k}_2, \mathbf{q} \\ s=\uparrow, \downarrow}} v_{\mathbf{q}} c_{\mathbf{k}_1 + \mathbf{q}}^{s\dagger} d_{\mathbf{k}_2 - \mathbf{q}}^\dagger d_{\mathbf{k}_2}^s c_{\mathbf{k}_1}^s \quad (4a)$$

and

$$V_{ee} = \frac{1}{2} \sum_{\substack{\mathbf{k}_1, \mathbf{k}_2, \mathbf{q} \\ s_1, s_2 = \uparrow, \downarrow}} v_{\mathbf{q}} c_{\mathbf{k}_1 + \mathbf{q}}^{s_1\dagger} c_{\mathbf{k}_2 - \mathbf{q}}^{s_2\dagger} c_{\mathbf{k}_2}^{s_2} c_{\mathbf{k}_1}^{s_1}, \quad (4b)$$

where $v_{\mathbf{q}} = \frac{2\pi e^2}{A\epsilon(q)}$ is the magnitude of the two-body interactions and $\epsilon(q)$ is a static dielectric function discussed in Sec. II C. The exciton-free electron elastic scattering matrix elements are henceforth defined as

$$V(\mathbf{q}, \mathbf{k}_e, \mathbf{k}_x) = \langle \mathbf{k}_x + \mathbf{q}, \mathbf{k}_e - \mathbf{q} | V | \mathbf{k}_x, \mathbf{k}_e \rangle. \quad (5)$$

Once matrix elements have been computed, the linewidth $\Gamma(n; \mathbf{k}_x)$ is calculated by summing over all final exciton states,

$$\Gamma(n, \mathbf{k}_x) = \frac{\hbar A}{(2\pi)^2} \int d^2q w(\mathbf{q}; n, \mathbf{k}_x). \quad (6)$$

Here, $w(\mathbf{q}; n, \mathbf{k}_x)$ is a partial scattering rate computed for fixed momentum transfer using Fermi's golden rule,

$$w(\mathbf{q}; n, \mathbf{k}_x) = \frac{2\pi}{\hbar} \sum_{\mathbf{k}_e} |V(\mathbf{q}, \mathbf{k}_e, \mathbf{k}_x)|^2 f(k_e) [1 - f(|\mathbf{k}_e - \mathbf{q}|)] \times \delta\left(\frac{\hbar^2 k_x^2}{2M_x} + \frac{\hbar^2 k_e^2}{2m_e} - \frac{\hbar^2 |\mathbf{k}_x + \mathbf{q}|^2}{2M_x} - \frac{\hbar^2 |\mathbf{k}_e - \mathbf{q}|^2}{2m_e}\right), \quad (7)$$

where the Fermi-Dirac distribution

$$f(k) = \left[e^{(\hbar^2 k^2 / 2m_e - \mu) / k_B T} + 1 \right]^{-1} \quad (8)$$

contains doping-density (n) dependence through the chemical potential $\mu = k_B T \ln[\exp \varepsilon_F / k_B T - 1]$ and the Fermi energy of a 2D electron gas, $\varepsilon_F = \pi \hbar^2 n / m_e$. In order to simplify the calculations, the parameter $\mathbf{k}_x = 0$ is taken in all computations, effectively choosing a reference frame in which the exciton is at rest. For further details, we refer the reader to Ref. 43, where similar calculations are performed for anisotropic 3D systems.

B. Electron-trion scattering

Computation of the trion-free electron elastic scattering linewidth contribution is similar to that of the excitonic case in all ways except for the determination of the scattering matrix elements. The trion-free electron scattering state is constructed similarly to that of (2), with a few key distinctions to be noted below. Explicitly, we write this scattering state as

$$|\mathbf{k}_t, \mathbf{k}_e\rangle = \sum_{\substack{\mathbf{k}_1, \mathbf{k}_2 \\ s_1, s_2, s_e}} \xi_S^*(s_1, s_2) \Phi_{\alpha_t, \mathbf{k}_t + \mathbf{k}_1, \alpha_t, \mathbf{k}_1 + \mathbf{k}_2}^* \psi_{\mathbf{k}_e}^* c_{-\mathbf{k}_1}^{s_1 \dagger} c_{-\mathbf{k}_2}^{s_2 \dagger} d_{\mathbf{k}_1 + \mathbf{k}_1 + \mathbf{k}_2}^\dagger c_{\mathbf{k}_e}^{s_e \dagger} |0\rangle. \quad (9)$$

Note the introduction of a spin wave function that constrains the trion to the singlet spin configuration, $\xi_S(s_1, s_2) = \langle s_1 s_2 | S \rangle$, via the projection of a two-fermion spin state $\langle s_1 s_2 |$ on the singlet state $|S\rangle$. The projection satisfies the properties $\sum_{s_1, s_2} \xi_S^*(s_1, s_2) \xi_S(s_1, s_2) = \langle S | S \rangle = 1$, and $\xi_S(s_1, s_2) = -\xi_S(s_2, s_1)$ as per Fermionic anti-commutation rules. Given that the trion triplet state is, at most, weakly bound, we consider only singlet to singlet scattering.

The trion wave function, Φ , is given by

$$\Phi_{\mathbf{k}_1, \mathbf{k}_2} = \mathcal{N} \frac{8\pi\lambda_1\lambda_2}{A} g(\lambda_1 k_1) g(\lambda_2 k_2). \quad (10)$$

Here, λ_1 and λ_2 are variational parameters associated with the Chandrasekhar-type wave function,^{18,47} and the constant \mathcal{N} is a normalization factor,

$$\mathcal{N} = \frac{1}{\sqrt{1 + \kappa^2}}, \quad \kappa = \frac{4\lambda_1\lambda_2}{(\lambda_1 + \lambda_2)^2}, \quad (11)$$

that arises during the variational minimization of the trion binding energy.⁴⁸

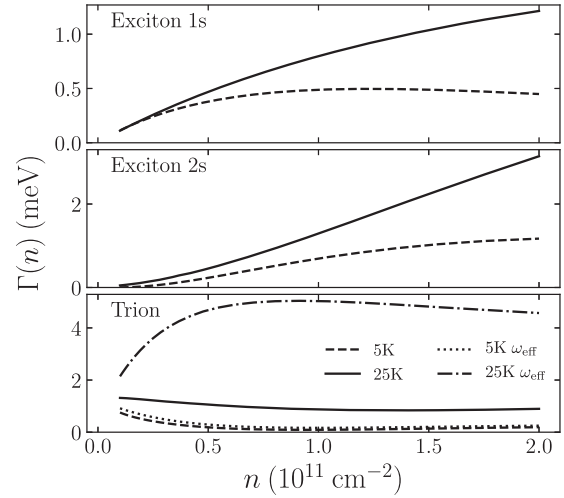


FIG. 1. Linewidth broadening of monolayer MoSe₂ as a function of electron doping density for BN-encapsulated ($\epsilon_0 = 4.5$)⁶¹ monolayers. The following parameters were used: in the exciton calculation, the effective Bohr radii $\lambda_0 = 10.3$ and in the case of the trion, $\lambda_1 = \lambda_0$ and $\lambda_2 = 25.2$ Å.¹⁸ In the exciton 2s elastic scattering, $a = 7.79$ Å and $b = 6.20$ Å (see Appendix B 4). The electron (hole) effective masses employed were 0.49 (0.61) (in units of m_0),⁶² and the polarizability was $\chi_{2D} = 8.23$ Å.¹⁸ In the case of exciton elastic scattering, the singlet and triplet contributions are identical as the exchange contribution to the potential dominates; trion triplet states are not considered. Additionally, screening using the effective frequency-dependent dielectric function [see Eq. (16)] are presented for the trion, as effective screening does not appear to affect the exciton linewidth.

Once the matrix elements

$$V(\mathbf{q}, \mathbf{k}_e, \mathbf{k}_t) = \langle \mathbf{k}_t + \mathbf{q}, \mathbf{k}_e - \mathbf{q} | V | \mathbf{k}_t, \mathbf{k}_e \rangle \quad (12)$$

are computed, the trion linewidth may be determined using (6) and (7) in the same way as for the exciton case (with the appropriate substitutions, e.g., the initial QP momentum $\mathbf{k}_x \rightarrow \mathbf{k}_t$, the mass ratio $\alpha_x \rightarrow \alpha_t = m_e / M_t$, etc.). Linewidths for low doping densities are reported in Sec. III, computational details of this calculation are given in Appendix D, and the physical parameters used may be found in the caption of Fig. 1.

C. Dielectric function

The dielectric function $\varepsilon(q, \omega)$ takes into account properties of the monolayer TMDC, the surrounding medium, and the excess electron gas,⁴⁹ respectively, and may be broken down into distinct contributions as⁵⁰

$$\varepsilon(q, \omega) = \varepsilon_I(q) + \varepsilon_{II}(q, \omega). \quad (13)$$

We follow previous work⁵¹ and screen the direct and exchange interactions, in contrast to the usual Bethe-Salpeter treatment of bound state formation where the exchange interaction is unscreened.^{52–55}

The first term consists of a static contribution from the monolayer TMDC and surrounding layers in the absence of doping,

$$\varepsilon_I(q) = \varepsilon_0(1 + 2\pi\chi_{2D}q), \quad (14)$$

where $\varepsilon_0 = (\varepsilon_a + \varepsilon_b)/2$ is the dielectric constant of the surrounding medium^{45,46} (the average of the two encapsulating dielectrics) and χ_{2D} is the dielectric polarizability of the 2D material.

The second term is due to the presence of doping electrons and is generally frequency dependent. We follow Stern⁴⁹ and treat the excess electrons as a 2D homogeneous electron gas (HEG). In the static ($\omega = 0$) approximation, this yields

$$\varepsilon_{II}(q, 0) = \frac{2me^2}{\hbar^2q} \begin{cases} 1 & \text{if } q \leq 2k_F \\ 1 - \sqrt{1 - (2k_F/q)^2} & \text{if } q > 2k_F. \end{cases} \quad (15)$$

Note that (15) implicitly carries a doping density (n) dependence through the Fermi momentum $p_F = \hbar k_F = \hbar\sqrt{2\pi n}$.

To motivate this choice, we observe that $\varepsilon(q, 0)$ captures the correct behavior in both the small-wavelength and low-doping limits. In the low-doping limit, the Stern-like term vanishes and the dielectric function $\varepsilon(q, 0) \rightarrow \varepsilon_I(q)$, which is the dielectric function of the material and its surroundings. The low q -limit suppresses the term containing the polarizability and diverges like $1/q$, correctly screening the 2D Coulomb interaction at small q .⁵⁶

If doping levels are large enough, the static approximation presented above will fail.^{56,57} Although this signals one aspect of the high doping density breakdown of the golden rule, one way to potentially extend its domain of validity is to utilize a frequency-dependent scattering matrix element as discussed in Ref. 51. This leads to a dielectric function derived from the 2D Lindhard function, $\varepsilon_{II}(q, E_{\text{eff}}/\hbar)$,^{49,51} evaluated at the effective energy

$$E_{\text{eff}} \equiv E(k_e) - E(|\mathbf{k}_e - \mathbf{q}|) = \frac{\hbar^2(2\mathbf{k}_e \cdot \mathbf{q} - q^2)}{2m_0}, \quad (16)$$

which is the energy difference between the initial and final states of the scattering electron. The details of $\varepsilon_{II}(q, \omega)$ are presented in Ref. 49 and in Appendix A.

III. RESULTS AND DISCUSSION

The Fermi golden rule is expected to be valid only in the ultra-low doping regime ($\varepsilon_F \ll \varepsilon_t \sim 10^{12} \text{ cm}^{-2}$), where ε_t denotes the trion binding energy in the limit of zero doping. As the doping level increases, many-body, multi-scattering effects become prominent,⁵⁸ and a Fermi-polaron-like picture appears to be required.^{35,37,38} Since the low-doping regime is now potentially controllable and accessible in encapsulated samples with graphene gating layers, a golden rule approach is useful in enabling a fully microscopic treatment in this restricted regime.

Linewidths vs doping level for both the exciton and trion lines are displayed for 5 K and 25 K in Fig. 1. Results are presented for the experimentally relevant case of a layer encapsulated by dielectric media with properties mimicking those of boron nitride. We also note that in a hypothetical suspended sample ($\varepsilon_0 = 1$), Γ is enhanced compared to results presented in Fig. 1 (e.g., roughly

5 meV at 10^{11} cm^{-2} , compared to only 1 meV in the encapsulated case) and is comparable to, or even larger than, that associated with phonon-induced broadening, since the scaling of Γ with respect to the background dielectric function varies roughly as ε_0^{-2} . It should also be noted that in experiments the encapsulating layers are of finite thickness, and while this situation can be handled theoretically,^{59,60} we do not do so here as it complicates the treatment of the dielectric function. We thus expect the true magnitude of linewidth values to be somewhat larger than the values presented in Fig. 1. Additionally, while we have also carried out an investigation of inelastic electron-capture scattering, we find that elastic scattering dominates the linewidths in the regimes we consider. Thus, we only focus on the elastic scattering contributions.

We first discuss trion line broadening. For doping levels $n > 0.4 \times 10^{11} \text{ cm}^{-2}$, the trion linewidth in all cases is largely independent of doping density. The upturn seen in the static screening trion linewidth as doping density decreases is likely an artifact of behavior embedded in the function $\varepsilon_2(q)$. Indeed, a suppression of the q^{-3} behavior for large q of this function leads to an essentially flat trion linewidth as a function of doping level, similar to that seen in Fermi-polaron-like theories and in some experiments.^{63,64} It should be noted that in these approaches, however, the trion line broadening is controlled by a phenomenological input parameter. For example, the width of the doping-independent trion line in the work of Efimkin and MacDonald³⁸ is given by the parameter γ , which is input phenomenologically by hand, is not derived directly from the microscopic interactions in the system.

Here, our fully microscopic approach allows for the microscopic extraction of the magnitude and temperature dependence of the trion linewidth. While the static and effective frequency-dependent screening cases are largely in agreement at low T , the same cannot be said for results at 25 K. Given the subtle changes in the scattering matrix elements except at small q , this difference likely arises from the larger accessible density of states available at higher densities away from $\omega = 0$ in the screening function.

We now turn to the broadening of the exciton line. Unlike the trion case, the exciton linewidth monotonically increases as a function of doping density at low values of n in the 25 K case. This is again in agreement with experimental expectations⁶⁵⁻⁶⁷ as well as the behavior found in many-body approaches.^{35,38,58} In particular, in these latter theoretical approaches, an approximately linear dependence of the linewidth on doping manifests over a much wider doping density range for the exciton line. The very same behavior arises from the golden rule at extremely low doping. The decrease of the slope of the linewidth as n increases, most clearly demonstrated in the near-plateau of the 5 K exciton linewidths above $n = 0.8 \times 10^{11} \text{ cm}^{-2}$, is a signature of the breakdown of the golden rule. Specifically, due to the $\varepsilon_F/k_B T$ term in the Fermi-Dirac distribution function, the crossover from the non-degenerate to the degenerate electron gas limit will induce a change in the doping dependence of the excitonic linewidth from a linear scaling $\Gamma \sim n$ at low doping to an eventual plateau $\sim k_B T$, and then an unphysical decline with increasing n . This same trend is reported in Ref. 43 for the quantum well case. We systematically examine this behavior in Fig. 2, which shows the doping and temperature dependence of this behavior. If one focuses on the more physically described regime $n < 0.8 \times 10^{11} \text{ cm}^{-2}$, it is observed that, unlike in the trion case, doping-induced exciton line broadening is largely insensitive to

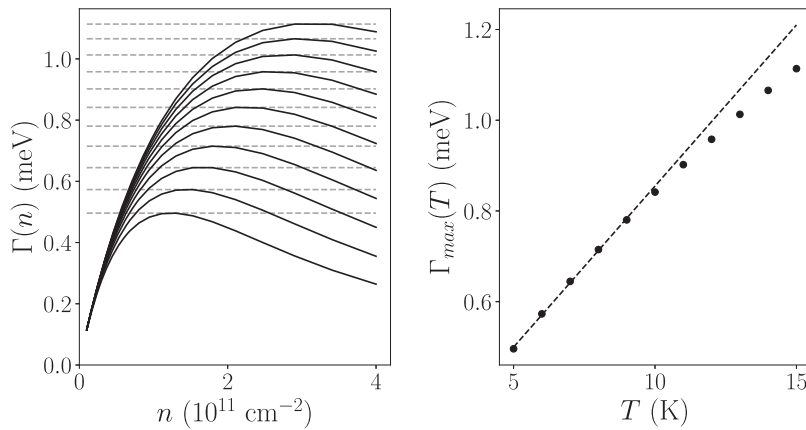


FIG. 2. Doping dependence of the 1s exciton linewidth at temperatures $T = 5, 6, \dots, 15$ K (left). Parameters describe monolayer MoSe_2 , as seen in Fig. 1. Lower linewidths correspond to lower temperatures. The horizontal dashed lines show the plateau location. The value of the maximum (plateau) is also plotted as a function of temperature, showing a clearly linear behavior at low T (right).

temperature variations in the range $T = 5\text{--}25$ K. Furthermore, given the fact that phonon-induced line broadening is suppressed at these temperatures, doping-induced line broadening effects may be observable at $T = 5$ K in clean, encapsulated samples even for doping densities as low as $n \sim 2 \times 10^{11} \text{ cm}^{-2}$, especially with respect to the 2s line, where the line broadening effects appear to be slightly enhanced compared to the ground state.

IV. CONCLUSION

In this work, we have employed perturbation theory to calculate the rates of electron–exciton and electron–trion scattering in monolayer TMDCs in the low doping density limit. Our approach is fully microscopic with respect to all input parameters and functions, including matrix elements and the dielectric screening model. On the other hand, it is expected that the Fermi golden rule should break down at low doping densities close to the degeneracy crossover of the electron gas in the monolayer, and some caution must be exercised with respect to the use of the forms of the dielectric screening functions employed here.⁵⁶ Avoiding these approximations allows for the description of a much broader range of doping but requires a full frequency-dependent many-body treatment.^{35,37,38}

Accepting the above limitations, the calculations presented here still allow for some important conclusions to be drawn. First, we find that with a reasonable treatment dielectric environment, exciton linewidths arising from exciton–electron scattering on the order of 1 meV or higher are possible at low temperatures in the low-doping regime accessible in encapsulated, graphene-gated samples. Thus, even mild doping may provide a line broadening mechanism that can compete with (but not necessarily exceed) lifetime and phonon-related broadening in this regime. As expected from previous many-body calculations in the very low-doping regime, the growth of the excitonic linewidth is monotonic with increasing n , while the trion linewidth is largely insensitive to doping. However, we find that the trion linewidth is sensitive to temperature variations even over the small range $T = 5\text{--}25$ K, a somewhat unexpected feature from the standpoint of many-body theories such as that of Ref. 38 where the trion linewidth is partly described by a phenomenological input parameter. Lastly, we find that excited state exciton line

broadening is somewhat larger and shows more sensitivity to increases in doping levels. Future work should be devoted to testing the veracity of these predictions and to understand how they merge with many-body approaches that have been applied to study the higher doping density regime.⁶⁸

In conclusion, we have provided a microscopic model for understanding how the scattering of excitons and trions surrounded by an electron gas in monolayer TMDCs may induce line broadening in the very low-doping density limit at low temperatures. A more detailed effort aimed at placing these contributions in the context of other mechanisms, such as exciton–phonon scattering, is worthy of future study. In addition, the approach adopted here may be of use for the calculation of the rates of processes such as Auger recombination^{69–71} in dimensionally confined systems. These and related topics will be the subject of future investigations.

ACKNOWLEDGMENTS

M.R.C. acknowledges support from the United States Department of Energy through the Computational Sciences Graduate Fellowship (DOE CSGF) under Grant No. DE-FG02-97ER25308. D.R.R. acknowledges support by Grant No. NSF-CHE 1464802. The authors acknowledge fruitful discussions with Ian S. Dunn, Timothy C. Berkelbach, Guy Ramon, Archana Raja, Alexey Chernikov, and Mikhail Glazov.

APPENDIX A: RPA POLARIZABILITY

Following the definition in Stern,⁴⁹ in this appendix, we present the frequency-dependent 2D electron gas polarizability, χ , and its $\omega \rightarrow 0$ limit. The general form of χ is $\chi(q, \omega) = \chi_1(q, \omega) + i\chi_2(q, \omega)$, where

$$\chi_1(z, \tilde{u}) = \frac{e^2 m}{\hbar^2 q^2 \pi} \left\{ 1 - \frac{C_-(z, \tilde{u})}{2} \sqrt{(1 - \tilde{u})^2 - z^{-2}} - \frac{C_+(z, \tilde{u})}{2} \sqrt{(1 + \tilde{u})^2 - z^{-2}} \right\} \quad (\text{A1})$$

and

$$\chi_2(z, \tilde{u}) = \frac{e^2 m}{\hbar^2 q^2 \pi} \left\{ \frac{D_-(z, \tilde{u})}{2} \sqrt{z^{-2} - (1 - \tilde{u})^2} - \frac{D_+(z, \tilde{u})}{2} \sqrt{z^{-2} - (1 + \tilde{u})^2} \right\}, \quad (\text{A2})$$

where $z \equiv q/2k_F$ and $\tilde{u} \equiv 2\omega m/\hbar q^2$. Note that the quantities in the braces, $\{\cdot\}$, are dimensionless. The functions C and D are defined as follows:

$$C_{\pm}(z, \tilde{u}) \equiv \begin{cases} (z \pm \tilde{u})/|z \pm \tilde{u}| & \text{if } |z \pm \tilde{u}| > 1 \\ 0 & \text{otherwise} \end{cases} \quad (\text{A3})$$

and

$$D_{\pm}(z, \tilde{u}) \equiv \begin{cases} 0 & \text{if } |z \pm \tilde{u}| > 1 \\ 1 & \text{otherwise.} \end{cases} \quad (\text{A4})$$

In the static approximation, we note that $\chi_2(q, 0) = 0$ and χ_1 reduces to (15), where generally

$$\varepsilon_2(q, \omega) = 2\pi B(q, \omega) \chi(q/2k_F, 2\omega m/\hbar q^2), \quad (\text{A5})$$

and $B(q, \omega) = \sqrt{q^2 - \varepsilon_0 \omega^2 c^{-2}}$.

APPENDIX B: EXCITON-ELECTRON ELASTIC SCATTERING

In this appendix, we outline the details of the $X + e^- \rightarrow X + e^-$ scattering calculation, including accounting for electron spin. Here, and in Appendix C, we closely follow the approach of Ref. 43, generalizing to the strict 2D limit and filling in necessary details.

In the following, it will be useful to keep in mind the electron and hole anti-commutation relations

$$\{d_{\mathbf{k}}^{s\dagger}, c_{\mathbf{k}'}^{s'\dagger}\} = \{d_{\mathbf{k}}^{s\dagger}, c_{\mathbf{k}'}^{s'}\} = \{d_{\mathbf{k}}^s, c_{\mathbf{k}'}^{s'\dagger}\} = \{d_{\mathbf{k}}^s, c_{\mathbf{k}'}^{s'}\} = 0$$

(electrons and holes always anti-commute) and

$$\{x_{\mathbf{k}}^s, x_{\mathbf{k}'}^{s'}\} = \{x_{\mathbf{k}}^{s\dagger}, x_{\mathbf{k}'}^{s'\dagger}\} = 0; \quad \{x_{\mathbf{k}}^s, x_{\mathbf{k}'}^{s'\dagger}\} = \delta_{\mathbf{k}\mathbf{k}'} \delta_{ss'},$$

where $x = c, d$. Moreover, recall that $\psi_{\mathbf{k}_c}$ ends up as a global phase factor in the expression for the scattering rate and will be ignored in the following derivations.

1. General form of the matrix elements

A prudent first step to computing (5) is to split up V into its constituent parts and evaluate them independently on the initial state $|\mathbf{k}_x, \mathbf{k}_e^{\beta}\rangle$, where spin indexes have been added as superscripts

(the exciton spin references the electron; hole spin will not be important). In the case of the electron-hole component, we have

$$V_{\text{eh}}|\mathbf{k}_x, \mathbf{k}_e^{\beta}\rangle = \sum_{\mathbf{k}'\mathbf{q}'} v_{q'} \phi^* \underbrace{c_{-\mathbf{k}'+\mathbf{q}'}^{\alpha\dagger} d_{\mathbf{k}_x+\mathbf{k}'-\mathbf{q}'}^{\dagger}}_{\text{self-interaction}} c_{\mathbf{k}_e}^{\beta\dagger} |0\rangle - \sum_{\mathbf{k}'\mathbf{q}'} v_{q'} \phi^* c_{-\mathbf{k}'}^{\alpha\dagger} d_{\mathbf{k}_x+\mathbf{k}'-\mathbf{q}'}^{\dagger} c_{\mathbf{k}_e+\mathbf{q}'}^{\beta\dagger} |0\rangle, \quad (\text{B1})$$

where $\phi^* \equiv \phi_{\alpha_x, \mathbf{k}_x+\mathbf{k}'}$. The first term in the above equation only contains information about the exciton interacting with itself (self-interaction) and is therefore discarded. The electron-electron component is calculated in a similar fashion and does not contain self-interaction terms,

$$V_{\text{ee}}|\mathbf{k}_x, \mathbf{k}_e^{\beta}\rangle = \sum_{\mathbf{k}'\mathbf{q}'} v_{q'} \phi^* c_{-\mathbf{k}'-\mathbf{q}'}^{\alpha\dagger} d_{\mathbf{k}_x+\mathbf{k}'}^{\dagger} c_{\mathbf{k}_e+\mathbf{q}'}^{\beta\dagger} |0\rangle. \quad (\text{B2})$$

From here, by direct computation, we find the general matrix elements of the electron-exciton elastic scattering process to be

$$\langle (\mathbf{k}_x + \mathbf{q})^{\theta}, (\mathbf{k}_e - \mathbf{q})^{\omega} | V_{\text{eh}} | \mathbf{k}_x, \mathbf{k}_e^{\beta} \rangle = - \sum_{\mathbf{k}''\mathbf{k}'\mathbf{q}'} \phi_1 \phi_2^* v_{q'} (\delta_{\mathbf{k}'', \mathbf{k}'}^{\theta\alpha} \delta_{\mathbf{q}, -\mathbf{q}'}^{\omega\beta} - \delta_{-\mathbf{k}'', \mathbf{k}_e+\mathbf{q}}^{\theta\beta} \delta_{\mathbf{k}_x, \mathbf{k}_e-\mathbf{q}}^{\omega\alpha}), \quad (\text{B3})$$

where $\phi_1 \phi_2^* \equiv \phi_{\alpha_x, \mathbf{k}_x+\alpha_x\mathbf{q}+\mathbf{k}''} \phi_{\alpha_x, \mathbf{k}_x+\mathbf{k}'}$. Explicitly, this is

$$\langle (\mathbf{k}_x + \mathbf{q})^{\theta}, (\mathbf{k}_e - \mathbf{q})^{\omega} | V_{\text{eh}} | \mathbf{k}_x, \mathbf{k}_e^{\beta} \rangle = v_q \delta_{\theta\alpha} \delta_{\omega\beta} \sum_{\mathbf{k}'} \phi_{\alpha_x, \mathbf{k}_x+\alpha_x\mathbf{q}+\mathbf{k}'} \phi_{\alpha_x, \mathbf{k}_x+\mathbf{k}'} - \phi_{\alpha_x, \mathbf{k}_x-\mathbf{k}_e+\mathbf{q}} \delta_{\theta\beta} \delta_{\omega\alpha} \sum_{\mathbf{k}'} \phi_{\alpha_x, \mathbf{k}_x+\alpha_x\mathbf{q}-\mathbf{k}_e-\mathbf{k}'} v_{k'}, \quad (\text{B4})$$

which can be separated into direct (corresponding to v_q) and exchange ($v_{k'}$) contributions. It is also observed that for practical computations, $\phi = \phi^*$ and thus the complex conjugation is dropped. The electron-electron term is computed as

$$\langle (\mathbf{k}_x + \mathbf{q})^{\theta}, (\mathbf{k}_e - \mathbf{q})^{\omega} | V_{\text{ee}} | \mathbf{k}_x, \mathbf{k}_e^{\beta} \rangle = \sum_{\mathbf{k}''\mathbf{k}'\mathbf{q}'} \phi_1 \phi_2^* v_{q'} (\delta_{\mathbf{k}'', \mathbf{k}'+\mathbf{q}'}^{\theta\alpha} \delta_{\mathbf{q}, -\mathbf{q}'}^{\omega\beta} - \delta_{-\mathbf{k}'', \mathbf{k}_e+\mathbf{q}}^{\theta\beta} \delta_{-\mathbf{k}'-\mathbf{q}', \mathbf{k}_e-\mathbf{q}}^{\omega\alpha}) \quad (\text{B5})$$

and simplified in a similar fashion,

$$\langle (\mathbf{k}_x + \mathbf{q})^{\theta}, (\mathbf{k}_e - \mathbf{q})^{\omega} | V_{\text{ee}} | \mathbf{k}_x, \mathbf{k}_e^{\beta} \rangle = v_q \delta_{\theta\alpha} \delta_{\omega\beta} \sum_{\mathbf{k}'} \phi_{\alpha_x, \mathbf{k}_x-\beta_x\mathbf{q}+\mathbf{k}'} \phi_{\alpha_x, \mathbf{k}_x+\mathbf{k}'} - \delta_{\theta\beta} \delta_{\omega\alpha} \times \sum_{\mathbf{k}'} \phi_{\alpha_x, \mathbf{k}_x+\alpha_x\mathbf{q}-\mathbf{k}_e-\mathbf{k}'} \phi_{\alpha_x, \mathbf{k}_x+\mathbf{q}-\mathbf{k}_e-\mathbf{k}'} v_{k'}. \quad (\text{B6})$$

Combining terms into direct and exchange contributions, we have

$$V^D(\mathbf{q}, \mathbf{k}_e, \mathbf{k}_x) = v_q \delta_{\theta\alpha} \delta_{\omega\beta} \sum_{\mathbf{k}'} \phi_{\alpha_x, \mathbf{k}_x+\mathbf{k}'} [\phi_{\alpha_x, \mathbf{k}_x-\beta_x\mathbf{q}+\mathbf{k}'} - \phi_{\alpha_x, \mathbf{k}_x+\alpha_x\mathbf{q}+\mathbf{k}'}], \quad (\text{B7})$$

where the Kronecker delta functions ensure that the proper spins are paired, and

$$V^{\text{XC}}(\mathbf{q}, \mathbf{k}_e, \mathbf{k}_x) = -\delta_{\theta\beta}\delta_{\omega\alpha} \sum_{\mathbf{k}'} v_{\mathbf{k}'} \phi_{\alpha, \mathbf{q}-\Delta\mathbf{k}_x+\mathbf{k}'} [\phi_{\mathbf{q}-\Delta\mathbf{k}_x+\mathbf{k}'} - \phi_{\mathbf{q}-\Delta\mathbf{k}_x}], \quad (\text{B8})$$

where $\Delta\mathbf{k}_x \equiv \mathbf{k}_e - \alpha_x \mathbf{k}_x$.

2. Spin contributions

Both the V_{ee} and V_{eh} terms can be split into clear direct and exchange contributions such that in the individual electron spin basis,

$$\langle \theta\omega | V | \alpha\beta \rangle = \delta_{\theta\alpha}\delta_{\omega\beta} V^{\text{D}} + \delta_{\theta\beta}\delta_{\omega\alpha} V^{\text{XC}}.$$

If the incident and exciton electrons are in a singlet configuration, we have to consider all contributions from the singlet state $|S\rangle = (|\uparrow\downarrow\rangle - |\downarrow\uparrow\rangle)/\sqrt{2}$,

$$\langle S | V | S \rangle = \frac{1}{2} (\langle \uparrow\downarrow | V | \uparrow\downarrow \rangle + \text{cc.} - \langle \uparrow\downarrow | V | \downarrow\uparrow \rangle - \text{cc.}),$$

which in the specified basis is

$$V_S \equiv \langle S | V | S \rangle = V^{\text{D}} - V^{\text{XC}}.$$

By inspection, any of the triplet configurations are

$$V_T \equiv \langle T | V | T \rangle = V^{\text{D}} + V^{\text{XC}}.$$

In the case of the exciton case, the singlet and triplet contributions are essentially identical since the exchange contribution dominates, meaning $|V_S|^2 \approx |V_T|^2$; for the trion, we do not consider triplet states.

3. 1s → 1s scattering

With the assumption that the exciton wave function ϕ is in the parameterized ground state (1s) given by (3), the direct interaction has an analytic form. Noting that

$$\sum_{\mathbf{k}} \rightarrow \frac{A}{(2\pi)^2} \int d^2k, \quad \mathbf{k} \in \mathbb{R}^2,$$

and that the convolution

$$\int d^2k' g(\lambda k') g(\lambda' |\mathbf{q} \pm \mathbf{k}'|) = \frac{2\pi}{(\lambda + \lambda')^2} g\left(\frac{\lambda\lambda'q}{\lambda + \lambda'}\right), \quad (\text{B9})$$

the direct terms simplify to (dropping the spin Kronecker deltas)

$$V_{1s}^{\text{D}}(q) = \frac{2\pi e^2}{Aq\epsilon(q)} [g(\lambda\beta_x q/2) - g(\lambda\alpha_x q/2)]. \quad (\text{B10})$$

The exchange terms do not simplify and must be evaluated numerically,

$$V_{1s}^{\text{XC}}(\mathbf{q}, \mathbf{k}_e, \mathbf{k}_x) = -\frac{4e^2\lambda^2}{A} \int \frac{d^2k'}{k'\epsilon(k')} g(\lambda|\alpha_x\mathbf{q} - \Delta\mathbf{k}_x + \mathbf{k}') \times [g(\lambda|\mathbf{k}_1 + \mathbf{q} - \Delta\mathbf{k}_x) - g(\lambda|\mathbf{q} - \Delta\mathbf{k}_x)]. \quad (\text{B11})$$

These results have been previously derived for scattering in finite quantum wells⁴³ and match the results above in the 2D analytic limit. Here, $\lambda = \lambda_0 = 10.3 \text{ \AA}$ is the exciton effective Bohr radius, and

$\alpha_x = m_e/M_x$ is the mass ratio of the exciton, $\beta_x = 1 - \alpha_x$, $m_e = 0.49m_0$ and $M_x = m_e + m_h$, where $m_h = 0.61m_0$.

4. 2s → 2s scattering

To compute the excited state (2s) exciton elastic scattering linewidth, we parameterize a radial 2s hydrogen wave function,

$$\phi^{2s}(r, a, b) \propto \left(2 - \frac{r}{b}\right) e^{-r/2a}, \quad (\text{B12})$$

in terms of an effective Bohr radius a and a secondary parameter b chosen to ensure orthogonality to the 1s state. An initial fit to the first excited state exact-diagonalization result of the Wannier exciton in a 2D Keldysh potential yielded length scales $a = 7.79 \text{ \AA}$ and $b = 5.33 \text{ \AA}$, the latter of which was modified to $b = 6.20 \text{ \AA}$ to ensure orthogonality. Fourier transforming to momentum-space yields

$$\phi_k^{2s} = N_{2s} \left[\frac{16\pi a^2}{(1 + 4a^2 k^2)^{3/2}} - \frac{2\pi(\frac{1}{2a^2} - k^2)}{b(\frac{1}{4a^2} + k^2)^{5/2}} \right] \quad (\text{B13})$$

with the normalization

$$N_{2s} = \sqrt{\frac{b^2}{4\pi a^2 A(3a^2 - 4ab + 2b^2)}}.$$

Matrix elements are computed by making the substitution $\phi \rightarrow \phi^{2s}$ in (B7) and (B8) and numerically performing the 2D integrals.

APPENDIX C: TRION-ELECTRON ELASTIC SCATTERING

The details of the $T + e^- \rightarrow T + e^-$ scattering process are significantly more involved than the exciton case. The introduction of an extra electron manifests as another pair of creation and annihilation operators in the matrix element evaluation and adds many more terms. While the calculation is longer, it is no more conceptually difficult. In this appendix, we present the detailed derivation of the matrix elements for a 2D system, which coincide with the results for the 3D quantum well in the $L \rightarrow 0$ limit.⁴³

The total elastic scattering matrix element $\mathcal{V}(\mathbf{q}, \mathbf{k}_e, \mathbf{k}_t)$ is calculated by first computing the action of $V|\mathbf{k}_t, \mathbf{k}_e\rangle$. This not only simplifies the number of operator contractions, but it also allows for the removal of self-interaction terms (those characterized by internal interactions between electrons and holes within the trion), as they do not contribute to the scattering matrix elements (similar to that of the exciton scattering case). To begin, we first evaluate the general contraction, which is used during the evaluation of (12),

$$c_1 c_2^\dagger c_3^\dagger c_4^\dagger |0\rangle = [\delta_{12} c_3^\dagger c_4^\dagger - \delta_{13} c_2^\dagger c_4^\dagger + \delta_{14} c_2^\dagger c_3^\dagger] |0\rangle, \quad (\text{C1})$$

where in (C2), $1 \equiv (\mathbf{k}'_1, z'_1, s'_1)$, $2 \equiv (-\mathbf{k}_1, z_1, s_1)$, $3 \equiv (-\mathbf{k}_2, z_2, s_2)$, and $4 \equiv (\mathbf{k}_e, z_e, s_e)$, as this will be useful in computing both $V_{eh}|\mathbf{k}_t, \mathbf{k}_e\rangle$ and $V_{ee}|\mathbf{k}_t, \mathbf{k}_e\rangle$. In following calculations, hole operators will be ignored, as they do not contribute additional constraints or prefactors to the linewidth calculations. Moreover, $V_{eh}|\mathbf{k}_t, \mathbf{k}_e\rangle$ evaluates to

$$\begin{aligned}
 V_{\text{eh}}|\mathbf{k}_t, \mathbf{k}_e\rangle &= - \sum_{\substack{\mathbf{k}_1, \mathbf{k}_2, \mathbf{k}'_1, \mathbf{q}' \\ s_1, s_2, s_e, s'_e}} u_{q'} \xi_S^*(s_1, s_2) \Phi_{\alpha_t, \mathbf{k}_t + \mathbf{k}_1, \alpha_t, \mathbf{k}_t + \mathbf{k}_2}^* \Psi_{\mathbf{k}_e}^* c_{\mathbf{k}'_1 + \mathbf{q}'}^{s'_1 \dagger} c_{\mathbf{k}'_1}^{s_1 \dagger} c_{-\mathbf{k}_2}^{s_2 \dagger} c_{\mathbf{k}_e}^{s_e \dagger} |0\rangle \\
 &= - \sum_{\substack{\mathbf{k}_1, \mathbf{k}_2, \mathbf{q}' \\ s_1, s_2, s_e}} \xi_S^*(s_1, s_2) \Phi_{\alpha_t, \mathbf{k}_t + \mathbf{k}_1, \alpha_t, \mathbf{k}_t + \mathbf{k}_2}^* \Psi_{\mathbf{k}_e}^* u_{q'} \left\{ c_{-\mathbf{k}_1 + \mathbf{q}'}^{s_1 \dagger} c_{-\mathbf{k}_2}^{s_2 \dagger} c_{\mathbf{k}_e}^{s_e \dagger} - c_{-\mathbf{k}_2 + \mathbf{q}'}^{s_1 \dagger} c_{-\mathbf{k}_1}^{s_2 \dagger} c_{\mathbf{k}_e}^{s_e \dagger} + c_{\mathbf{k}_e + \mathbf{q}'}^{s_1 \dagger} c_{-\mathbf{k}_1}^{s_2 \dagger} c_{-\mathbf{k}_2}^{s_e \dagger} \right\} |0\rangle.
 \end{aligned} \tag{C2}$$

The first two terms correspond to self-interactions between the internal electrons and holes of the trion. This is most easily seen by observing that after the action of V_{eh} on the trion-free electron state, the initial incident electron momentum \mathbf{k}_e remains unchanged in the final creation operator. In the last term, however, we see that a momentum exchange of \mathbf{q}' has taken place.

The electron–electron terms corresponding to $V_{\text{ee}}|\mathbf{k}_t, \mathbf{k}_e\rangle$ are calculated similarly. As in the electron–hole case, we begin by performing the right-most contraction

$$\begin{aligned}
 c_1 c_2 c_3^\dagger c_4^\dagger c_5^\dagger |0\rangle &= [\delta_{15} \delta_{24} - \delta_{14} \delta_{25}] c_3^\dagger |0\rangle \\
 &+ [\delta_{13} \delta_{25} - \delta_{15} \delta_{23}] c_4^\dagger |0\rangle \\
 &+ [\delta_{14} \delta_{23} - \delta_{13} \delta_{24}] c_5^\dagger |0\rangle,
 \end{aligned} \tag{C3}$$

where in (C3) and (C4) $1 \equiv (\mathbf{k}'_2, s'_2)$, $2 \equiv (\mathbf{k}'_1, s'_1)$, $3 \equiv (-\mathbf{k}_1, s_1)$, $4 \equiv (-\mathbf{k}_2, s_2)$, $5 \equiv (\mathbf{k}_e, s_e)$. In a similar fashion, $V_{\text{ee}}|\mathbf{k}_t, \mathbf{k}_e\rangle$ is thus found to be

$$\begin{aligned}
 V_{\text{ee}}|\mathbf{k}_t, \mathbf{k}_e\rangle &= \frac{1}{2} \sum_{\substack{\mathbf{k}_1, \mathbf{k}_2, \mathbf{k}'_1, \mathbf{k}'_2, \mathbf{q}' \\ s_1, s_2, s_e, s'_1, s'_2}} \xi_S^*(s_1, s_2) \Phi_{\alpha_t, \mathbf{k}_t + \mathbf{k}_1, \alpha_t, \mathbf{k}_t + \mathbf{k}_2}^* \Psi_{\mathbf{k}_e}^* u_{q'} c_{\mathbf{k}'_1 + \mathbf{q}'}^{s'_1 \dagger} c_{\mathbf{k}'_2 - \mathbf{q}'}^{s'_2 \dagger} c_{\mathbf{k}'_1}^{s_1 \dagger} c_{-\mathbf{k}_2}^{s_2 \dagger} c_{\mathbf{k}_e}^{s_e \dagger} |0\rangle \\
 &= \frac{1}{2} \sum_{\substack{\mathbf{k}_1, \mathbf{k}_2, \mathbf{q}' \\ s_1, s_2, s_e}} \xi_S^*(s_1, s_2) \Phi_{\alpha_t, \mathbf{k}_t + \mathbf{k}_1, \alpha_t, \mathbf{k}_t + \mathbf{k}_2}^* \Psi_{\mathbf{k}_e}^* u_{q'} \left\{ c_{-\mathbf{k}_2 + \mathbf{q}'}^{s_2 \dagger} c_{\mathbf{k}_e - \mathbf{q}'}^{s_e \dagger} c_{-\mathbf{k}_1}^{s_1 \dagger} - c_{\mathbf{k}_e + \mathbf{q}'}^{s_1 \dagger} c_{-\mathbf{k}_2 - \mathbf{q}'}^{s_2 \dagger} c_{-\mathbf{k}_1}^{s_e \dagger} \right. \\
 &+ \left. c_{\mathbf{k}_e + \mathbf{q}'}^{s_e \dagger} c_{-\mathbf{k}_1 - \mathbf{q}'}^{s_1 \dagger} c_{-\mathbf{k}_2}^{s_2 \dagger} - c_{-\mathbf{k}_1 + \mathbf{q}'}^{s_1 \dagger} c_{\mathbf{k}_e - \mathbf{q}'}^{s_e \dagger} c_{-\mathbf{k}_2}^{s_2 \dagger} + c_{-\mathbf{k}_1 + \mathbf{q}'}^{s_1 \dagger} c_{-\mathbf{k}_2 - \mathbf{q}'}^{s_2 \dagger} c_{\mathbf{k}_e}^{s_e \dagger} - c_{-\mathbf{k}_2 + \mathbf{q}'}^{s_2 \dagger} c_{-\mathbf{k}_1 - \mathbf{q}'}^{s_1 \dagger} c_{\mathbf{k}_e}^{s_e \dagger} \right\} |0\rangle \\
 &= \sum_{\substack{\mathbf{k}_1, \mathbf{k}_2, \mathbf{q}' \\ s_1, s_2, s_e}} \xi_S^*(s_1, s_2) \Phi_{\alpha_t, \mathbf{k}_t + \mathbf{k}_1, \alpha_t, \mathbf{k}_t + \mathbf{k}_2}^* \Psi_{\mathbf{k}_e}^* u_{q'} \left\{ c_{-\mathbf{k}_1}^{s_1 \dagger} c_{-\mathbf{k}_2 - \mathbf{q}'}^{s_2 \dagger} c_{\mathbf{k}_e + \mathbf{q}'}^{s_e \dagger} + c_{-\mathbf{k}_1 - \mathbf{q}'}^{s_1 \dagger} c_{-\mathbf{k}_2}^{s_2 \dagger} c_{\mathbf{k}_e + \mathbf{q}'}^{s_e \dagger} + c_{-\mathbf{k}_1 - \mathbf{q}'}^{s_1 \dagger} c_{-\mathbf{k}_2 + \mathbf{q}'}^{s_2 \dagger} c_{\mathbf{k}_e}^{s_e \dagger} \right\} |0\rangle.
 \end{aligned} \tag{C4}$$

In order to move from the second to the third equality in (C4), we have made use of the substitutions $\mathbf{q}' \rightarrow -\mathbf{q}'$ in the first, third, and fifth terms. The last term is a self-interaction exchange of momentum \mathbf{q}' between the two electrons on the trion.

With the self-interaction terms removed, and ignoring hole operators, the operation of $V = V_{\text{eh}} + V_{\text{ee}}$ acting on the trion–electron scattering state is

$$\begin{aligned}
 V|\mathbf{k}_t, \mathbf{k}_e\rangle &= \sum_{\substack{\mathbf{k}_1, \mathbf{k}_2, \mathbf{q}' \\ s_1, s_2, s_e}} \xi_S^*(s_1, s_2) \Phi_{\alpha_t, \mathbf{k}_t + \mathbf{k}_1, \alpha_t, \mathbf{k}_t + \mathbf{k}_2}^* \Psi_{\mathbf{k}_e}^* u_{q'} \\
 &\times \left\{ c_{-\mathbf{k}_1 - \mathbf{q}'}^{s_1 \dagger} c_{-\mathbf{k}_2}^{s_2 \dagger} + c_{-\mathbf{k}_1}^{s_1 \dagger} c_{-\mathbf{k}_2 - \mathbf{q}'}^{s_2 \dagger} - c_{-\mathbf{k}_1}^{s_1 \dagger} (z_1) c_{-\mathbf{k}_2}^{s_2 \dagger} \right\} c_{\mathbf{k}_e + \mathbf{q}'}^{s_e \dagger} |0\rangle.
 \end{aligned} \tag{C5}$$

The trion–electron elastic scattering matrix elements are given by the action of $\langle \mathbf{k}_t + \mathbf{q}, \mathbf{k}_e - \mathbf{q} |$ on (C5). Executing all possible integrals analytically produces a series of terms that can be broken into a direct component and two exchange components. We first adopt some notation: $\tilde{\lambda} = \lambda_1 \lambda_2 / (\lambda_1 + \lambda_2)$, is a harmonic-mean-like term that arises during convolutions, e.g., in (B9), and $\Delta \mathbf{k}_t = \mathbf{k}_e - \alpha_t \mathbf{k}_t$,

where \mathbf{k}_t is the initial trion momentum and $\alpha_t = m_e / M_t$ is the ratio of the effective electron mass to that of the trions $M_t = 2m_e + m_h$. Finally, the elastic scattering matrix elements, $\mathcal{V}(\mathbf{q}, \mathbf{k}_e, \mathbf{k}_t)$, are given by the sum of (C6) and (C8). The direct terms are

$$\mathcal{V}^{\text{D}}(q) = \frac{2\pi e^2}{q\epsilon(q)A(1 + \kappa^2)} \sum_{j=1}^5 g_j(q), \tag{C6}$$

where

$$\begin{aligned}
 g_1(q) &= g(\lambda_1 \alpha_t q / 2) g(\lambda_2 \beta_t q / 2), \\
 g_2(q) &= g(\lambda_2 \alpha_t q / 2) g(\lambda_1 \beta_t q / 2), \\
 g_3(q) &= 2\kappa^2 g(\tilde{\lambda} \alpha_t q) g(\tilde{\lambda} \beta_t q), \\
 g_4(q) &= -g(\lambda_1 \alpha_t q / 2) g(\lambda_2 \alpha_t q / 2), \\
 g_5(q) &= -\kappa^2 g^2(\tilde{\lambda} \alpha_t q)
 \end{aligned} \tag{C7}$$

and the exchange terms are

$$\mathcal{V}^{\text{XC}}(\mathbf{q}, \mathbf{k}_e, \mathbf{k}_t) = \frac{2e^2}{A(1 + \kappa^2)} \int \frac{d^2 k'}{k' \epsilon(k')} \sum_{j=1}^6 [G_j(\mathbf{q}, \mathbf{k}'; \lambda_1, \lambda_2) + G_j(\mathbf{q}, \mathbf{k}'; \lambda_2, \lambda_1)], \tag{C8}$$

where

$$\begin{aligned}
 G_1(\mathbf{q}, \mathbf{k}'; \lambda_1, \lambda_2) &= \lambda_2^2 g(\lambda_1 \alpha_t q/2) g(\lambda_2 |\Delta \mathbf{k}_t - \mathbf{q}|) g(\lambda_2 |\alpha_t \mathbf{q} - \Delta \mathbf{k}_t + \mathbf{k}'|), \\
 G_2(\mathbf{q}, \mathbf{k}'; \lambda_1, \lambda_2) &= -\lambda_2^2 g(\lambda_2 |\alpha_t \mathbf{q} - \Delta \mathbf{k}_t + \mathbf{k}'|) g(\lambda_1 |\alpha_t \mathbf{q} - \mathbf{k}'/2|) g(\lambda_2 |\Delta \mathbf{k}_t - \mathbf{q}|), \\
 G_3(\mathbf{q}, \mathbf{k}'; \lambda_1, \lambda_2) &= -\lambda_2^2 g(\lambda_1 \alpha_t q/2) g(\lambda_2 |\mathbf{q} - \Delta \mathbf{k}_t + \mathbf{k}'|) g(\lambda_2 |\alpha_t \mathbf{q} - \Delta \mathbf{k}_t + \mathbf{k}'|), \\
 G_4(\mathbf{q}, \mathbf{k}'; \lambda_1, \lambda_2) &= \kappa \lambda_1 \lambda_2 g(\tilde{\lambda} \alpha_t q) g(\lambda_1 |\alpha_t \mathbf{q} - \Delta \mathbf{k}_t + \mathbf{k}'|) g(\lambda_2 |\Delta \mathbf{k}_t - \mathbf{q}|), \\
 G_5(\mathbf{q}, \mathbf{k}'; \lambda_1, \lambda_2) &= -\kappa \lambda_1 \lambda_2 g(\lambda_1 |\alpha_t \mathbf{q} - \Delta \mathbf{k}_t + \mathbf{k}'|) g(\tilde{\lambda} |\alpha_t \mathbf{q} - \mathbf{k}'|) g(\lambda_2 |\Delta \mathbf{k}_t - \mathbf{q}|), \\
 G_6(\mathbf{q}, \mathbf{k}'; \lambda_1, \lambda_2) &= -\kappa \lambda_1 \lambda_2 g(\tilde{\lambda} \alpha_t q) g(\lambda_2 |\mathbf{q} - \Delta \mathbf{k}_t + \mathbf{k}'|) g(\lambda_1 |\alpha_t \mathbf{q} - \Delta \mathbf{k}_t + \mathbf{k}'|).
 \end{aligned} \tag{C9}$$

Applying $\langle \mathbf{k}_t + \mathbf{q}, \mathbf{k}_e - \mathbf{q} \rangle$ on (C5) produces a series of integrals, many of which may be evaluated analytically. In addition, the signs, and in some cases the prefactor, of the various terms are determined by summing over the spin degrees of freedom.

As in previous calculations, it is helpful to evaluate the contraction of Fermionic operators

$$\begin{aligned}
 \langle 0 | c_1 c_2 c_3 c_4^\dagger c_5^\dagger c_6^\dagger | 0 \rangle &= \delta_{16} (\delta_{34} \delta_{25} - \delta_{24} \delta_{35}) + \delta_{15} (\delta_{24} \delta_{36} - \delta_{34} \delta_{26}) \\
 &+ \delta_{14} (\delta_{35} \delta_{26} - \delta_{25} \delta_{36}),
 \end{aligned} \tag{C10}$$

where for the electron–hole interaction,

$$\begin{aligned}
 1 &\equiv (\mathbf{k}_e - \mathbf{q}, s'_e), \\
 2 &\equiv (-\mathbf{k}'_2, s'_2), \\
 3 &\equiv (-\mathbf{k}'_1, s'_1), \\
 4 &\equiv (-\mathbf{k}_1, s_1), \\
 5 &\equiv (-\mathbf{k}_2, s_2), \\
 6 &\equiv (\mathbf{k}_e + \mathbf{q}', s_e).
 \end{aligned} \tag{C11}$$

As an example, the terms including δ_{16} produce $g_4(q)$ and $g_5(q)$ in (C7), and the remainder of the exchange terms correspond to G_1 and G_4 in (C9).

To evaluate the first (second) electron–electron interactions, we replace $\mathbf{k}_1 \rightarrow \mathbf{k}_1 + \mathbf{q}'$ ($\mathbf{k}_2 \rightarrow \mathbf{k}_2 + \mathbf{q}'$) in (C11). Each of the six terms generated by the contraction in (C10) is evaluated individually for the hole and two electrons, generating 18 total terms and producing (C7) and (C9). Note that $g_3(q)$ in (C7) accounts for two identical electron–electron interaction terms.

Instead of presenting a derivation of all 18 terms, we present a detailed derivation of one of them. The others follow similarly. Consider the electron–hole term corresponding to $\delta_{24} \delta_{15} \delta_{36}$,

$$\begin{aligned}
 &-\frac{1}{2} \sum_{\substack{\mathbf{k}_1, \mathbf{k}_2, \mathbf{k}'_1, \mathbf{k}'_2, \mathbf{q}' \\ s_1, s_2, s_e, s'_1, s'_2, s'_e}} v_{q'} \xi_S^*(s_1, s_2) \xi_S(s'_1, s'_2) \psi_{\mathbf{k}_e}^* \psi_{\mathbf{k}_e - \mathbf{q}} \\
 &\times \Phi_{\alpha_t \mathbf{k}_t + \mathbf{k}_1, \alpha_t \mathbf{k}_t + \mathbf{k}_2}^* \Phi_{\alpha_t (\mathbf{k}_t + \mathbf{q}) + \mathbf{k}'_1, \alpha_t (\mathbf{k}_t + \mathbf{q}) + \mathbf{k}'_2} \\
 &\times \delta_{\mathbf{k}'_2, \mathbf{k}_1} \delta_{s'_2, s_1} \delta_{\mathbf{k}_e - \mathbf{q}, -\mathbf{k}_2} \delta_{s'_e, s_2} \delta_{-\mathbf{k}'_1, \mathbf{k}_e + \mathbf{q}'} \delta_{s'_1, s_e}.
 \end{aligned} \tag{C12}$$

Note that the factor of 1/2 is due to an average over the initial free-electron spin states. We may sum over the dummy variables $s'_1, s'_2, s'_e, \mathbf{k}'_2, \mathbf{k}_2$ and \mathbf{q}' . This yields

$$\begin{aligned}
 &-\frac{1}{2} \sum_{\substack{\mathbf{k}_1, \mathbf{k}'_1 \\ s_1, s_2, s_e}} v_{\mathbf{k}_e + \mathbf{k}'_1} \xi_S^*(s_1, s_2) \xi_S(s_e, s_1) \psi_{\mathbf{k}_e}^* \psi_{\mathbf{k}_e - \mathbf{q}} \\
 &\times \Phi_{\alpha_t \mathbf{k}_t + \mathbf{k}_1, \alpha_t \mathbf{k}_t + \mathbf{q} - \mathbf{k}_e}^* \Phi_{\alpha_t (\mathbf{k}_t + \mathbf{q}) + \mathbf{k}'_1, \alpha_t (\mathbf{k}_t + \mathbf{q}) + \mathbf{k}_1}.
 \end{aligned} \tag{C13}$$

The spin factors are evaluated first,

$$\sum_{s_1, s_2, s_e} \xi_S^*(s_1, s_2) \xi_S(s_e, s_1) = \begin{cases} -1 & \text{if } s_2 = s_e \\ 0 & \text{if } s_2 \neq s_e. \end{cases} \tag{C14}$$

After sorting each term in (C13) by an integration variable and making the substitutions $\mathbf{k}'_1 \rightarrow \mathbf{k}'_1 - \mathbf{k}_e$ and $\mathbf{k}_1 \rightarrow \mathbf{k}_1 - \alpha_t \mathbf{k}_t$, one integral may be evaluated analytically using the convolution in (B9), yielding $G_4(\mathbf{q}, \mathbf{k}'; \lambda_1, \lambda_2)$ after the substitution $\Delta \mathbf{k}_t = \mathbf{k}_e - \alpha_t \mathbf{k}_t$ is made.

APPENDIX D: COMPUTATIONAL DETAILS

All integrations were performed using the Cubature adaptive integration package.⁷² Integrals over $(0, \infty)$ were mapped to the finite range $(0, 1)$ and performed using adaptive integration. Additionally, in order to avoid exhausting available memory, integrals were nested in the following way: First, scattering matrix elements were computed on the fly and converged to some relative error tolerance ϵ . This results in a computation of a 2D integral for the exchange terms. Once the matrix element V is computed, the golden rule integration that contains $|V|^2$, along with the integration over all final states, is performed (this is a three-dimensional integral) and converged to some error tolerance $c\epsilon$, where c is typically on the order of 100–1000. Finally, to ensure convergence, the entire computation is converged with respect to the decrease in ϵ .

DATA AVAILABILITY

The data that support the findings of this study are available from the corresponding author upon reasonable request.

REFERENCES

- K. F. Mak, C. Lee, J. Hone, J. Shan, and T. F. Heinz, *Phys. Rev. Lett.* **105**, 136805 (2010).
- A. Splendiani, L. Sun, Y. Zhang, T. Li, J. Kim, C.-Y. Chim, G. Galli, and F. Wang, *Nano Lett.* **10**, 1271 (2010).
- K. S. Novoselov, A. K. Geim, S. V. Morozov, D. Jiang, Y. Zhang, S. V. Dubonos, I. V. Grigorieva, and A. A. Firsov, *Science* **306**, 666 (2004).
- K. S. Novoselov, A. K. Geim, S. Morozov, D. Jiang, M. Katsnelson, I. Grigorieva, S. Dubonos, and A. A. Firsov, *Nature* **438**, 197 (2005).

- ⁵K. P. Loh, Q. Bao, G. Eda, and M. Chhowalla, *Nat. Chem.* **2**, 1015 (2010).
- ⁶G. Wang, A. Chernikov, M. M. Glazov, T. F. Heinz, X. Marie, T. Amand, and B. Urbaszek, *Rev. Mod. Phys.* **90**, 021001 (2018).
- ⁷T. C. Berkelbach and D. R. Reichman, *Annu. Rev. Condens. Matter Phys.* **9**, 379 (2018).
- ⁸Z. Cai, B. Liu, X. Zou, and H.-M. Cheng, *Chem. Rev.* **118**, 6091 (2018).
- ⁹M. Chhowalla, H. S. Shin, G. Eda, L.-J. Li, K. P. Loh, and H. Zhang, *Nat. Chem.* **5**, 263 (2013).
- ¹⁰N. Flöry, A. Jain, P. Bharadwaj, M. Parzefall, T. Taniguchi, K. Watanabe, and L. Novotny, *Appl. Phys. Lett.* **107**, 123106 (2015).
- ¹¹S. Memaran, N. R. Pradhan, Z. Lu, D. Rhodes, J. Ludwig, Q. Zhou, O. Ogunsolu, P. M. Ajayan, D. Smirnov, A. I. Fernández-Domínguez *et al.*, *Nano Lett.* **15**, 7532 (2015).
- ¹²S. Wi, M. Chen, D. Li, H. Nam, E. Meyhofer, and X. Liang, *Appl. Phys. Lett.* **107**, 062102 (2015).
- ¹³Q. H. Wang, K. Kalantar-Zadeh, A. Kis, J. N. Coleman, and M. S. Strano, *Nat. Nanotechnol.* **7**, 699 (2012).
- ¹⁴D. Ovchinnikov, A. Allain, Y.-S. Huang, D. Dumcenco, and A. Kis, *ACS Nano* **8**, 8174 (2014).
- ¹⁵D. Lembke, S. Bertolazzi, and A. Kis, *Acc. Chem. Res.* **48**, 100 (2015).
- ¹⁶D. Y. Qiu, H. Felipe, and S. G. Louie, *Phys. Rev. Lett.* **111**, 216805 (2013).
- ¹⁷F. Wu, F. Qu, and A. H. MacDonald, *Phys. Rev. B* **91**, 075310 (2015).
- ¹⁸T. C. Berkelbach, M. S. Hybertsen, and D. R. Reichman, *Phys. Rev. B* **88**, 045318 (2013).
- ¹⁹K. F. Mak, K. He, C. Lee, G. H. Lee, J. Hone, T. F. Heinz, and J. Shan, *Nat. Mater.* **12**, 207 (2013).
- ²⁰T. Cheiwchanamngaj and W. R. Lambrecht, *Phys. Rev. B* **85**, 205302 (2012).
- ²¹A. Chernikov, T. C. Berkelbach, H. M. Hill, A. Rigosi, Y. Li, O. B. Aslan, D. R. Reichman, M. S. Hybertsen, and T. F. Heinz, *Phys. Rev. Lett.* **113**, 076802 (2014).
- ²²K. He, N. Kumar, L. Zhao, Z. Wang, K. F. Mak, H. Zhao, and J. Shan, *Phys. Rev. Lett.* **113**, 026803 (2014).
- ²³G. Plechinger, P. Nagler, J. Kraus, N. Paradiso, C. Strunk, C. Schüller, and T. Korn, *Phys. Status Solidi RRL* **9**, 457 (2015).
- ²⁴M. Currie, A. Hanbicki, G. Kioseoglou, and B. Jonker, *Appl. Phys. Lett.* **106**, 201907 (2015).
- ²⁵A. Mittoğlu, P. Plochocka, J. Jadczyk, W. Escoffier, G. Rikken, L. Kulyuk, and D. Maude, *Phys. Rev. B* **88**, 245403 (2013).
- ²⁶G. Moody, C. K. Dass, K. Hao, C.-H. Chen, L.-J. Li, A. Singh, K. Tran, G. Clark, X. Xu, G. Berghäuser *et al.*, *Nat. Commun.* **6**, 8315 (2015).
- ²⁷M. Selig, G. Berghäuser, A. Raja, P. Nagler, C. Schüller, T. F. Heinz, T. Korn, A. Chernikov, E. Malic, and A. Knorr, *Nat. Commun.* **7**, 13279 (2016).
- ²⁸O. A. Ajayi, J. V. Ardelean, G. D. Shepard, J. Wang, A. Antony, T. Taniguchi, K. Watanabe, T. F. Heinz, S. Strauf, X. Zhu *et al.*, *2D Mater.* **4**, 031011 (2017).
- ²⁹F. Cadiz, E. Courtade, C. Robert, G. Wang, Y. Shen, H. Cai, T. Taniguchi, K. Watanabe, H. Carrere, D. Lagarde *et al.*, *Phys. Rev. X* **7**, 021026 (2017).
- ³⁰S. Shree, A. George, T. Lehnert, C. Neumann, M. Benelajla, C. Robert, X. Marie, K. Watanabe, T. Taniguchi, U. Kaiser *et al.*, *2D Mater.* **7**, 015011 (2019).
- ³¹D. Christiansen, M. Selig, G. Berghäuser, R. Schmidt, I. Niehues, R. Schneider, A. Arora, S. M. de Vasconcellos, R. Bratschitsch, E. Malic *et al.*, *Phys. Rev. Lett.* **119**, 187402 (2017).
- ³²K. Shinokita, X. Wang, Y. Miyauchi, K. Watanabe, T. Taniguchi, and K. Matsuda, *Adv. Funct. Mater.* **29**, 1900260 (2019).
- ³³Y. Miyauchi, S. Konabe, F. Wang, W. Zhang, A. Hwang, Y. Hasegawa, L. Zhou, S. Mouri, M. Toh, G. Eda *et al.*, *Nat. Commun.* **9**, 2598 (2018).
- ³⁴B. R. Carvalho, L. M. Malar, J. M. Alves, C. Fantini, and M. A. Pimenta, *Phys. Rev. Lett.* **114**, 136403 (2015).
- ³⁵M. Sidler, P. Back, O. Cotlet, A. Srivastava, T. Fink, M. Kroner, E. Demler, and A. Imamoglu, *Nat. Phys.* **13**, 255 (2017).
- ³⁶P.-F. Li and Z.-W. Wang, *J. Appl. Phys.* **123**, 204308 (2018).
- ³⁷Y.-W. Chang and D. R. Reichman, *Phys. Rev. B* **99**, 125421 (2019).
- ³⁸D. K. Efimkin and A. H. MacDonald, *Phys. Rev. B* **95**, 035417 (2017).
- ³⁹M. Klawunn and A. Recati, *Phys. Rev. A* **84**, 033607 (2011).
- ⁴⁰R. Schmidt, T. Enss, V. Pietilä, and E. Demler, *Phys. Rev. A* **85**, 021602 (2012).
- ⁴¹M. M. Parish and J. Levinsen, *Phys. Rev. A* **87**, 033616 (2013).
- ⁴²A. Lherbier, X. Blase, Y.-M. Niquet, F. Triozon, and S. Roche, *Phys. Rev. Lett.* **101**, 036808 (2008).
- ⁴³G. Ramon, A. Mann, and E. Cohen, *Phys. Rev. B* **67**, 045323 (2003).
- ⁴⁴J. Henriques, G. Ventura, C. Fernandes, and N. Peres, *J. Phys.: Condens. Matter* **32**, 025304 (2019).
- ⁴⁵N. S. Rytova, *Vestn. Mosk. Univ. Fiz. Astron.* **3**, 30 (1967).
- ⁴⁶L. Keldysh, *J. Exp. Theor. Phys. Lett.* **29**, 658 (1979).
- ⁴⁷S. Chandrasekhar, *Astrophys. J.* **100**, 176 (1944).
- ⁴⁸N. P. Sandler and C. R. Proetto, *Phys. Rev. B* **46**, 7707 (1992).
- ⁴⁹F. Stern, *Phys. Rev. Lett.* **18**, 546 (1967).
- ⁵⁰T. C. Berkelbach, "Two-dimensional screening for doped semiconductors" (unpublished).
- ⁵¹G. F. Giuliani and J. J. Quinn, *Phys. Rev. B* **26**, 4421 (1982).
- ⁵²G. Strinati, *Riv. Nuovo Cimento* **11**, 1 (1988).
- ⁵³M. Rohlfing and S. G. Louie, *Phys. Rev. B* **62**, 4927 (2000).
- ⁵⁴W. Hanke and L. Sham, *Phys. Rev. Lett.* **43**, 387 (1979).
- ⁵⁵L. X. Benedict, *Phys. Rev. B* **66**, 193105 (2002).
- ⁵⁶M. M. Glazov and A. Chernikov, *Phys. Status Solidi B* **255**, 1800216 (2018).
- ⁵⁷B. Scharf, D. Van Tuan, I. Žutić, and H. Dery, *J. Phys.: Condens. Matter* **31**, 203001 (2019).
- ⁵⁸Y.-C. Chang, S.-Y. Shiau, and M. Combescot, *Phys. Rev. B* **98**, 235203 (2018).
- ⁵⁹K. Andersen, S. Latini, and K. S. Thygesen, *Nano Lett.* **15**, 4616 (2015).
- ⁶⁰L. Cavalcante, A. Chaves, B. Van Duppen, F. Peeters, and D. Reichman, *Phys. Rev. B* **97**, 125427 (2018).
- ⁶¹P. J. Gielisse, S. S. Mitra, J. N. Plendl, R. D. Griffis, L. C. Mansur, R. Marshall, and E. A. Pascoe, *Phys. Rev.* **155**, 1039 (1967).
- ⁶²F. A. Rasmussen and K. S. Thygesen, *J. Phys. Chem. C* **119**, 13169 (2015).
- ⁶³G. Astakhov, V. Kochereshko, D. Yakovlev, W. Ossau, J. Nürnberger, W. Faschinger, and G. Landwehr, *Phys. Rev. B* **62**, 10345 (2000).
- ⁶⁴T. Smoleński, O. Cotlet, A. Popert, P. Back, Y. Shimazaki, P. Knüppel, N. Dietler, T. Taniguchi, K. Watanabe, M. Kroner *et al.*, *Phys. Rev. Lett.* **123**, 097403 (2019).
- ⁶⁵E. Courtade, M. Semina, M. Manca, M. Glazov, C. Robert, F. Cadiz, G. Wang, T. Taniguchi, K. Watanabe, M. Pierre *et al.*, *Phys. Rev. B* **96**, 085302 (2017).
- ⁶⁶Z. Ye, L. Waldecker, E. Y. Ma, D. Rhodes, A. Antony, B. Kim, X.-X. Zhang, M. Deng, Y. Jiang, Z. Lu *et al.*, *Nat. Commun.* **9**, 3718 (2018).
- ⁶⁷Recent unpublished experimental results by K. Wagner, E. Wietek, and J. Zipfel in the group of Alexey Chernikov have given access to linewidths as a function of doping in the low-doping regime in clean, encapsulated WSe₂ at 5 K. While the data fill in the upper end of the doping regime we present in our Fig. 1, they are in reasonable agreement with our results, including monotonically increasing (with doping level n) exciton lines of width 5–10 meV, a somewhat larger growth for the 2s line as compared to 1s, and a nearly flat trion line that initially slightly decreases with increasing n . We thank Alexey Chernikov for sharing these results to us after the submission of this work.
- ⁶⁸C. Fey, P. Schmelcher, A. Imamoglu, and R. Schmidt, [arXiv:1912.04873](https://arxiv.org/abs/1912.04873) (2019).
- ⁶⁹L. Huang and T. D. Krauss, *Phys. Rev. Lett.* **96**, 057407 (2006).
- ⁷⁰F. Wang, Y. Wu, M. S. Hybertsen, and T. F. Heinz, *Phys. Rev. B* **73**, 245424 (2006).
- ⁷¹F. Hu, C. Yin, H. Zhang, C. Sun, W. W. Yu, C. Zhang, X. Wang, Y. Zhang, and M. Xiao, *Nano Lett.* **16**, 6425 (2016).
- ⁷²S. G. Johnson, Cubature (Multi-dimensional integration), 2017, [http://ab-initio.mit.edu/wiki/index.php/Cubature_\(Multi-dimensional_integration\)](http://ab-initio.mit.edu/wiki/index.php/Cubature_(Multi-dimensional_integration)).